PCCP

COMMUNICATION

View Article Online
View Journal | View Issue

Cite this: *Phys. Chem. Chem. Phys.*, 2025, **27**, 16738

Received 2nd July 2025,
Accepted 16th July 2025

DOI: 10.1039/d5cp02520f

rsc.li/pccp

Cryogenic action spectroscopy of the cyan fluorescent protein chromophore anion†

Jordan Dezalay, [a] Eleanor K. Ashworth, [b] Jack E. Fulker, [a] Mark H. Stockett, [c] Jennifer A. Noble [a] and James N. Bull *[b]

Action spectroscopy at $T \approx 30$ K, as a proxy for the visible absorption band, and the branching between electron detachment and dissociation in the cyan fluorescent protein chromophore anion are reported. The cryogenic action spectra, which show the presence of several rotamers, serve as a reference point for interpreting the effect of nano-environmental interactions in complex protein environments. The adiabatic detachment energy for the lowest energy geometric isomer (*Z*1) is 19 531 ± 40 cm^{-1}, with the vertical $S_1 \leftarrow S_0$ transition energy at 23 734 ± 40 cm^{-1}. For *Z*1, the propensity for internal conversion followed by dissociation is low (<10%) compared with autodetachment as the $S_1 \leftarrow S_0$ absorption band is entirely situated in the detachment continuum and is classified as a shape resonance.

Fluorescent proteins (FPs) are the foundation stone for modern, high-resolution bioimaging of cells and the monitoring of microscopic biological processes.[1] Accordingly, a wide range of derivatives of FPs have been developed offering a full colour palette,[2–5] including cyan fluorescent protein (CFP).[6] For CFP, mutations over three generations of FPs have substantially improved quantum yield and other fluorescence properties,[7–9] allowing it to become a widespread biomarker. In several derivative CFPs, including NowGFP and mNeonGreen,[10,11] the chromophore may be deprotonated and probably resides as the anion (cyan$^-$). The optical properties of FPs are dictated by the chromophore unit embedded within a protein binding pocket, with the amalgamation of non-covalent interactions and the local electrostatic field leading to an electrochromic spectral shift and perturbation of the intrinsic photophysics of chromophores.[12,13] It is of fundamental importance to characterise the photophysics of FP chromophores in a 'bottom up' approach in order to understand the influence of the environment (solvent or protein)[14] and for calibrating or benchmarking of theory.[15]

The chromophore in CFP, shown in Fig. 1, is a tryptophan-based derivative of the well-known green fluorescent protein (GFP) chromophore. By probing FP chromophores in isolation (*i.e. in vacuo*), their intrinsic photophysics can be elucidated without the complications of solvent effects (*e.g.* solvatochromic shifts).[16] While the photophysics of the anionic GFP chromophore and substituted forms has been studied thoroughly in the gas phase using action spectroscopy techniques at $T \approx 300$ K,[17–25] and at cryogenic temperatures,[26–29] and is understood in the gas phase through *ab initio* molecular dynamics simulations,[15,30] the anionic CFP chromophore is

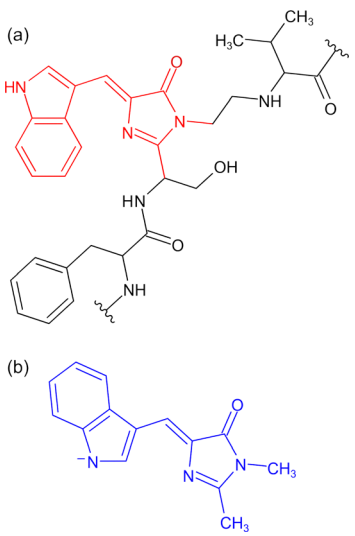

Fig. 1 (a) Structure of the cyan chromophore (red) within CFP, which adopts a *Z*2 rotamer (*i.e.* rotation about the central single bond) configuration due to an array of non-covalent interactions. (b) Lowest energy rotamer of isolated cyan$^-$ (blue), denoted as *Z*1, which has *Z*-isomer geometry about the methylene bond. For simplicity, we refer to all geometric isomers and rotamers (*Z*1, *Z*2, *E*1, and *E*2) as isomers. Structures of all isomers are summarised in the ESI.†

[a] *Aix-Marseille University, CNRS, PIIM, Marseille, France*
[b] *Chemistry, Faculty of Science, University of East Anglia, Norwich NR4 7TJ, UK. E-mail: james.bull@uea.ac.uk*
[c] *Department of Physics, Stockholm University, SE-10691 Stockholm, Sweden*

† Electronic supplementary information (ESI) available: Mass spectra demonstrating anion fragments, optimised geometries of possible cyan$^-$ isomers and rotamers. See DOI: https://doi.org/10.1039/d5cp02520f

largely unstudied apart from ion storage ring measurements[31,32] and room-temperature anion photoelectron spectroscopy.[33] It is valuable to perform clear gas-phase experiments on mutant GFP chromophores in order to understand structure–activity trends in the photoactive units of fluorescent proteins.

Here, we characterise the $S_1 \leftarrow S_0$ absorption band and adiabatic electron detachment threshold of isolated cyan$^-$ at $T \approx 30$ K using action spectroscopy, monitoring photoneutrals (parent and fragment neutrals). Our measurements used the cryogenic ion trap action spectroscopy apparatus at the PIIM laboratory (Aix-Marseille University),[34,35] where cyan$^-$ was generated through electrospray ionisation (at $T = 300$ K) of a 1 : 1 methanol–water solution with a trace amount of ammonia. Significantly, because the chromophore was synthesised stereospecifically as a *Z*-isomer,[25] it was assumed to be predominately the *Z* isomer in the gas phase based on the use of 'gentle' ion production conditions.[21] Electrosprayed ions were trapped in a 3D quadrupole ion trap cooled using a helium cryostat; several temperature sensors spread across the ion trap assembly measured temperatures ranging from 12 to 35 K,[36] with the contents of the trap expected at $T \approx 30$ K (the minimum temperature measured close to the cold head was $T = 21$ K). Since the action spectroscopy is dominated by electron detachment, with dissociation being a minor channel, we performed action spectroscopy monitoring parent and fragment neutrals. Here, trapped parent anions were extracted and irradiated (3.62 μs after extraction) with the laser radiation (EKSPLA NT-342B optical parametric oscillator, ≈6 cm^{-1} spectral resolution, calibrated with a wavemeter) in a Gauss tube as part of a time-of-fight region. Parent and fragment anions were decelerated, allowing neutral particles

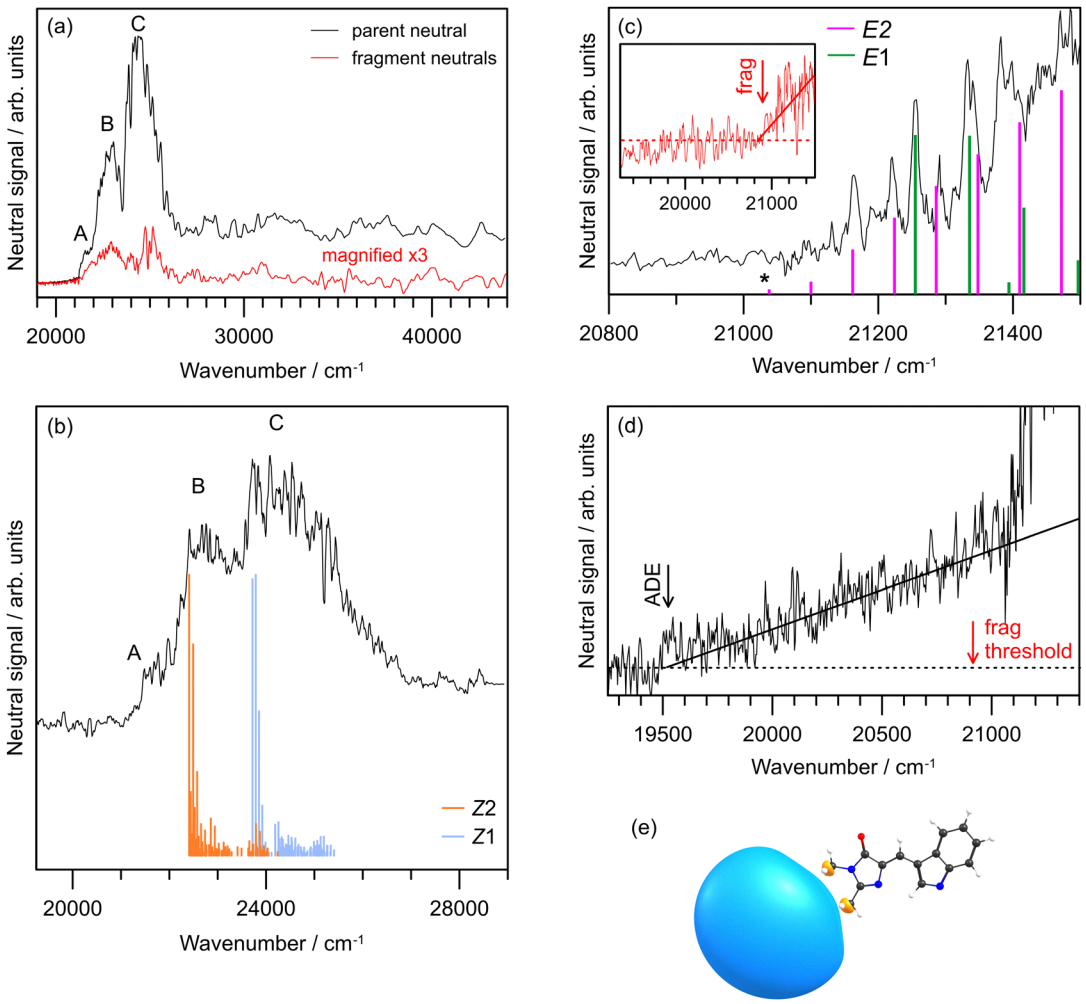

Fig. 2 Action spectra of cyan$^-$ recorded at $T \approx 30$ K: (a) complete spectra recorded for the parent neutral signal (black) and fragment neutrals (red), with a step size of 0.5 nm. (b) Higher resolution scan (black) over the main group of transitions, with a step size of 0.2 nm. Franck–Condon–Herzberg–Teller ($S_1 \leftarrow S_0$) simulations for the *Z*1 (blue) and *Z*2 (orange) isomers are shown and were translated so that respective 0–0 transitions match the onset of the two spectral bands. (c) Higher resolution scan (0.06 nm step size) over region A, assigned to the weak signal from *E*1 (green) and *E*2 (magenta) isomers. The inset corresponds to fragment neutrals, with a threshold extrapolated to ≈20 900 cm^{-1}. * Denotes the simulated hot-band signal from *E*1, which correlates with the fragment neutral threshold (see the inset). (d) Extrapolation of the parent neutral signal to the adiabatic detachment energy (ADE) threshold at 19 531 ± 40 cm^{-1}. No fragment neutral signal was detected for $h\nu < 20\,900$ cm^{-1} (see the inset in c). (e) Calculated DBS orbital for the *Z*1 isomer with an isosurface value of 0.005 a.u. and a binding energy of 41 meV (≈ 330 cm^{-1}).

to impact a microchannel plate detector. Because dissociation is accompanied by kinetic energy release (*i.e.* fragments moving away from each other), there is a change in the recorded time-of-flight (TOF) profile, allowing the fragment yield to be quantified by analysing laser-on against laser-off TOF profiles. Data were normalised relative to the laser-off signal and light fluence. A complete description of the experimental strategies is given in ref. 37.

To support assignments of the experimental spectra, quantum chemical calculations were performed. Geometries and vibrational frequencies were computed at the ωB97X-D/aug-cc-pVTZ level of theory[38,39] using Gaussian 16.B01,[40] while electron detachment energies and vertical excitation energies (VEEs) were computed at the DLPNO-CCSD(T)/aug-cc-pVTZ[41] and STEOM-DLPNO-CCSD/aug-cc-pVTZ[42] levels of theory using ORCA 6.0.1.[43] Absorption profiles ($S_1 \leftarrow S_0$ transition) were simulated using the Franck–Condon–Herzberg–Teller (FCHT) framework as implemented in Gaussian.[44] The dipole-bound state (DBS) was characterised using the EOM-CCSD/aug-cc-pVDZ + 8spd methodology, where +8spd is a series of uncontracted functions (orbital exponents $\zeta = 0.1$ to 2.91×10^{-5}, with a geometric progression ratio of 3.13)[45] situated ≈5 Å beyond the molecule along the dipole moment vector of the radical neutral (in the anion geometry).

Action spectra recorded over the 19 500–44 000 cm^{-1} (≈500–225 nm) range are shown in Fig. 2a. Parent neutrals were produced in much higher abundance than fragment neutrals across the studied spectral range, demonstrating that autodetachment is much more probable than photoexcitation followed by internal conversion and statistical dissociation. The spectra reveal three bands, labelled A, B, and C, which are present in both parent neutral and fragment neutral spectra. These were assigned as follows: A – *E*1 and *E*2 isomers, B – *Z*2 isomer, and C – *Z*1 isomer. This assignment is consistent with the band intensities and expected gas-phase populations (T = 300 K Boltzmann distribution followed by rapid cooling and kinetic trapping). Specifically, from the relative energies in Table 1, a ratio of 100 : 73 for *Z*1 : *Z*2 is predicted, which is in good agreement with the experimental band intensities. A small amount of *E*1 and *E*2 may be produced through collisions in low vacuum regions (the nascent population of *E*1 at T = 300 K is ≈3%).[21] Additionally, the ordering of computed VEEs (Table 1) is consistent with the band assignments. For each of the four isomers, the $S_1 \leftarrow S_0$ transition is bright (oscillator strength $f = 0.6$ for *Z*1), while the VEE for the $S_2 \leftarrow S_0$ transition is calculated in the range of 27 000–30 000 cm^{-1} but with $f \approx 10^{-2}$.

A higher resolution spectrum of the parent neutral over the $S_1 \leftarrow S_0$ transition is shown in Fig. 2b. There is no obvious vibrational structure, which is in parallel with observations for action spectra of protonated cations of cyan similarly recorded at $T \approx 20$ K. FCHT simulations predict the transitions for the *Z*1 and *Z*2 isomers to be origin dominated, although the overlap of spectra due to multiple isomers complicates an experiment–theory comparison. Our FCHT simulations, included in Fig. 2b, indicate the spectrum should be dominated by contributions from a ≈70 cm^{-1} mode (torsion of the single bond on the methylene bridge). This, combined with higher frequency combination bands and indole ring modes, lead to a congested spectral profile. An earlier room-temperature photoneutral spectrum of $cyan^-$ revealed a single peak with the wavelength of maximum response at ≈459 nm (≈21 790 cm^{-1}),[31] which is red shifted by ≈2000 cm^{-1} compared with the most intense band (C) present in the cryogenic spectrum (23 835 ± 50 cm^{-1}, Fig. 2). STEOM-DLPNO-CCSD calculations on excited states of the radical neutrals produced energies outside of our spectral window, consistent with no direct detachment channels that could account for bands A, B, or C. This result is consistent with the expected radical neutral excited states for the related green fluorescent protein chromophore anion.[20]

The parent neutral spectrum recorded over band A is shown in Fig. 2c, revealing a clear vibrational structure starting at ≈21 100 cm^{-1}. The spectral position of this vibrational structure was not consistent with any hot band simulations for the *Z*1 or *Z*2 isomers; the hot band signal extending from band C or B over band A would require ions with room temperature or warmer internal energies. However, FCHT simulations show that band A is consistent with small quantities of the *E*1 and *E*2 isomers (expected at ≈3% from an initial Boltzmann thermal population). The FCHT simulations show that the *E*1 isomer is dominated by the origin and first excited vibration of the ≈62 cm^{-1} torsion mode, although the *E*2 isomer shows an extended progression dominated by a 62 cm^{-1} mode, which is because of the steric hindrance and consequential non-planarity of the *E*2 isomer (leading to the highest E_{rel} value in Table 1), *i.e.* the excited state for *E*2 is non-planar. The inset in Fig. 2c shows that the weak signal associated with fragment neutrals is observed from ≈20 900 cm^{-1}, consistent with the assignment of band A to electronically excited anionic states rather than being linked with direct photodetachment processes. Assignments of the labelled vibrations in Fig. 2c are given in the ESI.†

While the fragment neutral signal threshold is ≈20 900 cm^{-1} (Fig. 2c, inset), the parent neutral threshold was extrapolated to a lower wavenumber of 19 531 ± 40 cm^{-1} (Fig. 2d), which defines the adiabatic detachment energy (ADE). We assign this value to the *Z*1 isomer since it is the most abundant gas phase species and because the calculated ADEs for each isomer (Table 1) indicate that *Z*1 appears at the lowest energy. The calculated value (Table 1) is ≈2600 cm^{-1} higher in energy. Since the direct photodetachment signal is so weak compared with autodetachment from the overlapping $S_1 \leftarrow S_0$ transition, it is not possible to discern a reliable

Table 1 Calculated energetics of each $cyan^-$ isomer (see the illustrations in the ESI). Relative energy (E_{rel}), vertical excitation energy (VEE) for the $S_1 \leftarrow S_0$ transition, and adiabatic and vertical detachment energies (ADE and VDE) are all given in cm^{-1}. Dipole moment magnitudes, $|\mu|$, are given in Debye

Species	E_{rel}	VEE	ADE	VDE	$\lvert\mu\rvert$
*Z*1	0	25 121	22 148	23 197	4.75
*Z*2	66	24 871	22 495	23 455	6.69
*E*1	720	24 759	22 301	23 197	6.10
*E*2	2013	24 994	22 648	23 479	6.49

VDE value. Room temperature photoelectron spectroscopy measurements on cyan$^-$ have shown VDE = 2.75 ± 0.02 eV (22 177 ± 161 cm^{-1}),[33] which is likely complicated by large autodetachment signals considering the photon energies chosen in that study. It is also worth noting that our fragment neutral signal threshold at ≈20 900 cm^{-1} is consistent with the critical energy threshold (kinetically shifted dissociation threshold) from a recent cryogenic ion storage ring study.[32]

TOF mass spectrometry confirmed that the neutral fragments, which are produced in low quantity (<10%) compared with the parent neutral signal, are linked with the production of anions with *m/z* 223 (–CH_3) and *m/z* 153 (likely involves intramolecular rearrangement), with the former being the predominant photofragmentation pathway for the GFP chromophore anions.[24,46] The bond dissociation energy (BDE) for the –CH_3 channel is ≈1.6 eV (≈12 900 cm^{-1}),[31] which is ≈6600 cm^{-1} below the adiabatic detachment threshold. We consequently expect that the small amount of S_1 population following photoexcitation that is able to internally convert to recover the ground electronics will undergo dissociation rather than thermionic emission. In turn, this implies that the parent neutral spectrum should be predominately from direct photodetachment and autodetachment processes.

It is worth noting that the parent neutral cores for each isomer of cyan have permanent dipole moments that support a (non-valence) DBS since $|\mu| > 2.5$ D (Table 1).[47,48] The calculated DBS orbital for the *Z*1 isomer is shown in Fig. 2e with a calculated binding energy of 41 meV (≈330 cm^{-1}). As expected, the orbital is localised in the direction of the positive end of the molecular dipole moment for the neutral core. Because the oscillator strength to excite the DBS is $f < 10^{-4}$, such states are only observed clearly, *e.g.* the ground vibrational state through two-photon detachment[49] or collisional detachment,[50,51] when the spectroscopic focus is not on nearby valence-localised states with oscillator strengths four to five orders of magnitude higher (*Z*1, $f \approx 0.6$ for the $S_1 \leftarrow S_0$ transition).[52,53] Furthermore, cryogenic action spectroscopy on deprotonated indole similarly showed no clear individual DBS transitions in the vicinity of the detachment threshold (rather a broad, unresolved distribution),[54] while other nitrogen-conditioning PAHs show clearly resolved DBS vibrations. We conclude that DBS transitions are very weak in cyan$^-$ action spectra, are swamped by the other excitation processes and are consequently not important in the action spectroscopy of cyan$^-$.

In some ways, the cryogenic action spectra of cyan$^-$ contrast with those recorded for the GFP chromophore anion. The latter may exist as *E* and *Z* geometric isomers in the gas phase,[21] but is not complicated by rotamers due to the symmetry of a *para*-phenoxide moiety rather than the deprotonated indole group in cyan$^-$. Moreover, the GFP case shows a clear vibrational structure with a pronounced ≈80 cm^{-1} progression assigned to the methine bridge bending/ring scissoring mode from FCHT simulations.[27,28] Significantly, in the case of the GFP chromophore anion, the $S_1 \leftarrow S_0$ absorption band extends over the detachment threshold with experiments showing differing electron detachment to dissociation branching occurring when tuning the laser wavenumber over the band due to a small excited state barrier (≈250 cm^{-1}) to an internal conversion coordinate.[26,28] This interpretation has been further evidenced by recent cryogenic gas-phase fluorescence measurements.[29] In contrast, for cyan$^-$, the electron detachment threshold (for *Z*1) is situated in the range of 1500–2000 cm^{-1} below the onset of the $S_2 \leftarrow S_1$ transition. Thus, the S_1 excited state in cyan, which is classified as a shape resonance, is entirely situated above the detachment threshold. In such a case, we expect the shape resonance lifetimes to be on the order of tens to hundreds of femtoseconds and, consequently, to show lifetime broadening.[16,55] On the other hand, the weak electron detachment signal associated with the *E*1 and *E*2 isomers (which is red-shifted compared with the *Z*-isomers and the *E*-isomers have higher calculated ADE values, Table 1) shows progression with simulated 62 cm^{-1} spacing, consistent with twisting of the methine bridge and the resolved vibrational structure due to the longer excited-state lifetime.

In summary, cryogenic action spectroscopy of cyan$^-$ has characterised the $S_1 \leftarrow S_0$ absorption properties of the *Z*1, *Z*2, *E*1 and *E*2 isomers and the adiabatic electron detachment thresholds for the *Z*1 isomer. The lack of a clear vibrational structure, for the major isomer, *Z*1, is attributed to some combination of congested vibronic transitions and lifetime broadening effects due to prompt autodetachment. The presence of two rotamers for the gas-phase anion is expected to translate to solution, although the abundance of each rotamer will depend on specific solvent-molecule interactions. Consequently, experimental studies of the chromophore in solution (*e.g.* using ultrafast pump-probe spectroscopies), will probe differing conformer distributions depending on if the pump excites on the red or blue edge of the absorption band.

Conflicts of interest

There are no conflicts to declare.

Data availability

The data that support the findings of this study are available from the corresponding author upon reasonable request.

Acknowledgements

This work was funded by an EPSRC New Investigator Award (EP/W018691 to J. N. B.), a project grant from the Olle Engkvist Foundation (200-0575 to M. H. S.), and the Swedish Foundation for International Cooperation in Research and Higher Education (STINT) Grant for Internationalisation programme (PT2017-7328 to M. H. S. and J. N. B.). E. K. A. thanks the University of East Anglia for a doctoral studentship.

References

1 *Fundamentals of Fluorescence Imaging*, ed. G. Cox, Jenny Stanford Publishing, 2019.
2 G.-J. Kremers, J. Goedhart, E. B. van Munster and T. W. J. Gadella, *Biochemistry*, 2006, **45**, 6570–6580.

3 G. D. Malo, L. J. Pouwels, M. Wang, A. Weichsel, W. R. Montfort, M. A. Rizzo, D. W. Piston and R. M. Wachter, *Biochemistry*, 2007, **46**, 9865–9873.
4 B. Seefeldt, R. Kasper, T. Seidel, P. Tinnefeld, K.-J. Dietz, M. Heilemann and M. Sauer, *J. Biophotonics*, 2008, **1**, 74–82.
5 J. S. Paige, K. Y. Wu and S. R. Jaffrey, *Science*, 2011, **333**, 642–646.
6 R. Heim, D. C. Prasher and R. Y. Tsien, *Proc. Natl. Acad. Sci. U. S. A.*, 1994, **91**, 12501–12504.
7 G. Gotthard, D. von Stetten, D. Clavel, M. Noirclerc-Savoye and A. Royant, *Biochemistry*, 2017, **56**, 6418–6422.
8 M. L. Markwardt, G.-J. Kremers, C. A. Kraft, K. Ray, P. J. C. Cranfill, K. A. Wilson, R. N. Day, R. M. Wachter, M. W. Davidson and M. A. Rizzo, *PLoS One*, 2011, **6**, e17896.
9 J. Goedhart, D. von Stetten, M. Noirclerc-Savoye, M. Lelimousin, L. Joosen, M. A. Hink, L. van Weeren, T. W. J. Gadella and A. Royant, *Nat. Commun.*, 2012, **3**, 751.
10 K. Sarkisyan, A. Goryashchenko, P. Lidsky, D. Gorbachev, N. Bozhanova, A. Gorokhovatsky, A. Pereverzeva, A. Ryumina, V. Zherdeva, A. Savitsky, K. Solntsev, A. Bommarius, G. Sharonov, J. Lindquist, M. Drobizhev, T. Hughes, A. Rebane, K. Lukyanov and A. Mishin, *Biophys. J.*, 2015, **109**, 380–389.
11 L. Zarowny, D. Clavel, R. Johannson, K. Duarte, H. Depernet, J. Dupuy, H. Baker, A. Brown, A. Royant and R. E. Campbell, *Protein Eng., Des. Sel.*, 2022, **35**, gzac004.
12 M. A. Steffen, K. Lao and S. G. Boxer, *Science*, 1994, **264**, 810–816.
13 M. Saggu, S. D. Fried and S. G. Boxer, *J. Phys. Chem. B*, 2019, **123**, 1527–1536.
14 A. Fatima, E. K. Ashworth, I. Chambrier, A. N. Cammidge, G. Bressan, S. R. Meech and J. N. Bull, *Phys. Chem. Chem. Phys.*, 2025, **27**, 9407–9416.
15 N. H. List, C. M. Jones and T. J. Martínez, *Chem. Sci.*, 2022, **13**, 373–385.
16 E. K. Ashworth, M.-H. Kao, C. S. Anstöter, G. Riesco-Llach, L. Blancafort, K. M. Solntsev, S. R. Meech, J. R. R. Verlet and J. N. Bull, *Phys. Chem. Chem. Phys.*, 2023, **25**, 23626–23636.
17 L. H. Andersen, H. Bluhme, S. Boyé, T. J. D. Jørgensen, H. Krogh, I. B. Nielsen, S. Brøndsted Nielsen and A. Svendsen, *Phys. Chem. Chem. Phys.*, 2004, **6**, 2617–2627.
18 M. W. Forbes and R. A. Jockusch, *J. Am. Chem. Soc.*, 2009, **131**, 17038–17039.
19 C. R. S. Mooney, M. E. Sanz, A. R. McKay, R. J. Fitzmaurice, A. E. Aliev, S. Caddick and H. H. Fielding, *J. Phys. Chem. A*, 2012, **116**, 7943–7949.
20 C. W. West, J. N. Bull, A. S. Hudson, S. L. Cobb and J. R. R. Verlet, *J. Phys. Chem. B*, 2015, **119**, 3982–3987.
21 E. Carrascosa, J. N. Bull, M. S. Scholz, N. J. A. Coughlan, S. Olsen, U. Wille and E. J. Bieske, *J. Phys. Chem. Lett.*, 2018, **9**, 2647–2651.
22 N. J. A. Coughlan, M. H. Stockett, C. Kjær, E. K. Ashworth, P. C. B. Page, S. R. Meech, S. B. Nielsen, L. Blancafort, W. S. Hopkins and J. N. Bull, *J. Chem. Phys.*, 2021, **155**, 124304.
23 J. L. Woodhouse, A. Henley, R. Lewin, J. M. Ward, H. C. Hailes, A. V. Bochenkova and H. H. Fielding, *Phys. Chem. Chem. Phys.*, 2021, **23**, 19911–19922.
24 E. K. Ashworth, M. H. Stockett, C. Kjaer, P. C. B. Page, S. R. Meech, S. B. Nielsen and J. N. Bull, *J. Phys. Chem. A*, 2022, **126**, 1158–1167.
25 E. K. Ashworth, J. Dezalay, C. R. M. Ryan, C. Ieritano, W. S. Hopkins, I. Chambrier, A. N. Cammidge, M. H. Stockett, J. A. Noble and J. N. Bull, *Phys. Chem. Chem. Phys.*, 2023, **25**, 20405–20413.
26 A. Svendsen, H. V. Kiefer, H. B. Pedersen, A. V. Bochenkova and L. H. Andersen, *J. Am. Chem. Soc.*, 2017, **139**, 8766–8771.
27 W. Zagorec-Marks, M. M. Foreman, J. R. R. Verlet and J. M. Weber, *J. Phys. Chem. Lett.*, 2019, **10**, 7817–7822.
28 L. H. Andersen, A. P. Rasmussen, H. B. Pedersen, O. B. Beletsan and A. V. Bochenkova, *J. Phys. Chem. Lett.*, 2023, **14**, 6395–6401.
29 T. T. Lindkvist, I. Djavani-Tabrizi, L. H. Andersen and S. B. Nielsen, *Phys. Rev. Lett.*, 2025, **134**, 093001.
30 N. H. List, C. M. Jones and T. J. Martínez, *Commun. Chem.*, 2024, **7**, 25.
31 S. Boyé, I. B. Nielsen, S. B. Nielsen, H. Krogh, A. Lapierre, H. B. Pedersen, S. U. Pedersen, U. V. Pedersen and L. H. Andersen, *J. Chem. Phys.*, 2003, **119**, 338–345.
32 J. Flotte de Pouzols, A. Subramani, E. K. Ashworth, J. N. Bull, H. Cederquist, J. Dezalay, N. H. List, P. Martini, J. E. N. Navarrete, H. T. Schmidt, H. Zettergren, B. Zhu and M. H. Stockett, *Phys. Rev. A*, 2025, **111**, 043112.
33 M. A. Parkes, A. Bennett and H. H. Fielding, *Mol. Phys.*, 2019, **117**, 3027–3035.
34 I. Alata, J. Bert, M. Broquier, C. Dedonder, G. Féraud, G. Grégoire, S. Soorkia, E. Marceca and C. Jouvet, *J. Phys. Chem. A*, 2013, **117**, 4420–4427.
35 J. A. Noble, E. Marceca, C. Dedonder, I. Carvin, E. Gloaguen and C. Jouvet, *Eur. Phys. J. D*, 2021, **75**, 1–13.
36 N. Esteves-López, C. Dedonder-Lardeux and C. Jouvet, *J. Chem. Phys.*, 2015, **143**, 074303.
37 G. A. Pino, R. A. Jara-Toro, J. P. Aranguren-Abrate, C. Dedonder-Lardeux and C. Jouvet, *Phys. Chem. Chem. Phys.*, 2019, **21**, 1797–1804.
38 J.-D. Chai and M. Head-Gordon, *Phys. Chem. Chem. Phys.*, 2008, **10**, 6615–6620.
39 T. H. Dunning, *J. Chem. Phys.*, 1989, **90**, 1007–1023.
40 M. J. Frisch, G. W. Trucks, H. B. Schlegel, G. E. Scuseria, M. A. Robb, J. R. Cheeseman, G. Scalmani, V. Barone, G. A. Petersson, H. Nakatsuji, X. Li, M. Caricato, A. V. Marenich, J. Bloino, B. G. Janesko, R. Gomperts, B. Mennucci, H. P. Hratchian, J. V. Ortiz, A. F. Izmaylov, J. L. Sonnenberg, D. Williams-Young, F. Ding, F. Lipparini, F. Egidi, J. Goings, B. Peng, A. Petrone, T. Henderson, D. Ranasinghe, V. G. Zakrzewski, J. Gao, N. Rega, G. Zheng, W. Liang, M. Hada, M. Ehara, K. Toyota, R. Fukuda, J. Hasegawa, M. Ishida, T. Nakajima, Y. Honda, O. Kitao, H. Nakai, T. Vreven, K. Throssell, J. A. Montgomery, Jr., J. E. Peralta, F. Ogliaro, M. J. Bearpark, J. J. Heyd, E. N. Brothers, K. N. Kudin, V. N. Staroverov, T. A. Keith, R. Kobayashi, J. Normand, K. Raghavachari, A. P. Rendell, J. C. Burant, S. S. Iyengar, J. Tomasi, M. Cossi, J. M. Millam, M. Klene, C. Adamo, R. Cammi, J. W. Ochterski, R. L. Martin, K. Morokuma,

O. Farkas, J. B. Foresman and D. J. Fox, *Gaussian 16 Revision B.01*, 2016, Gaussian Inc, Wallingford CT.
41 I. Sandler, J. Chen, M. Taylor, S. Sharma and J. Ho, *J. Phys. Chem. A*, 2021, **125**, 1553–1563.
42 A. K. Dutta, M. Saitow, B. Demoulin, F. Neese and R. Izsák, *J. Chem. Phys.*, 2019, **150**, 164123.
43 F. Neese, *WIREs Comput. Mol. Sci.*, 2011, **2**, 73–78.
44 F. Santoro, A. Lami, R. Improta, J. Bloino and V. Barone, *J. Chem. Phys.*, 2008, **128**, 224311.
45 P. Skurski, M. Gutowski and J. Simons, *Int. J. Quantum Chem*, 2000, **80**, 1024–1038.
46 S. B. Nielsen, A. Lapierre, J. U. Andersen, U. V. Pedersen, S. Tomita and L. H. Andersen, *Phys. Rev. Lett.*, 2001, **87**, 228102.
47 E. Fermi and E. Teller, *Phys. Rev.*, 1947, **72**, 399–408.
48 J. Simons, *J. Phys. Chem. A*, 2008, **112**, 6401–6511.
49 Y.-R. Zhang, D.-F. Yuan and L.-S. Wang, *J. Phys. Chem. Lett.*, 2023, **14**, 7368–7381.
50 J. N. Bull, J. T. Buntine, M. S. Scholz, E. Carrascosa, L. Giacomozzi, M. H. Stockett and E. J. Bieske, *Faraday Discuss.*, 2019, **217**, 34–46.
51 J. N. Bull, C. S. Anstöter, M. H. Stockett, C. J. Clarke, J. A. Gibbard, E. J. Bieske and J. R. R. Verlet, *J. Phys. Chem. Lett.*, 2021, **12**, 11811–11816.
52 E. K. Ashworth, S. H. Ashworth and J. N. Bull, *Rev. Sci. Instrum.*, 2024, **95**, 075103.
53 E. K. Ashworth and J. N. Bull, *J. Chem. Phys.*, 2024, **161**, 114302.
54 J. A. Noble, E. Marceca, C. Dedonder and C. Jouvet, *Phys. Chem. Chem. Phys.*, 2020, **22**, 27290–27299.
55 J. N. Bull, C. W. West and J. R. R. Verlet, *Chem. Sci.*, 2015, **6**, 1578–1589.